Observation of transverse patterns in an isotropic microchip laser

Y. F. Chen
Department of Electrophysics, National Chiao Tung University, Hsinchu, Taiwan, Republic of China

Y. P. Lan
Institute of Electro-Optical Engineering, National Chiao Tung University, Hsinchu, Taiwan, Republic of China

(Received 20 August 2002; published 22 April 2003)

An isotropic microchip laser is used to study the characteristics of high-order wave functions in a two-dimensional (2D) quantum harmonic oscillator based on the identical functional forms. With a doughnut pump profile, the spontaneous transverse modes are found to, generally, be elliptic and hyperbolic transverse modes. Theoretical analyses reveal that the elliptic transverse modes are analogous to the coherent states of a 2D harmonic oscillator; the formation of hyperbolic transverse modes is a spontaneous mode locking between two identical Hermite-Gaussian modes.

DOI: 10.1103/PhysRevA.67.043814 PACS number(s): 42.60.Jf, 42.55.Xi

I. INTRODUCTION

The quantum harmonic oscillator is an excellent pedagogical system to understand the basic properties of quantum mechanics. The eigenfunction of the two-dimensional (2D) quantum harmonic oscillator can be analytically expressed as Hermite-Gaussian (HG) function with Cartesian symmetry (x,y) or Laguerre-Gaussian (LG) function with cylindrical symmetry (r,ϕ) [1]. It is well known that the paraxial wave equation for the spherical laser resonators has the identical form with the Schrödinger equation for the 2D harmonic oscillator [2–4]. Since the functional forms of the 2D quantum oscillator and the spherical resonators are similar, the higher transverse modes of the spherical resonators can be in terms of HG modes or LG modes. Recently, the pure high-order HG modes and LG modes have been successfully generated from a microchip laser [5–7].

An usually elusive question in quantum mechanics is that of building high-order wave functions that mimics the familiar classical periodic orbits for two-dimensional (2D) and 3D quantum systems. Modern interest in this topic can, in part, be attributed to the continuous desire to attain a more thorough understanding of the quantum-classical connection in mesoscopic systems. For example, some striking phenomena in quantum ballistic cavities are found to be associated with the wave functions in terms of classical periodic orbits [8–10]. On the other hand, the semiclassical periodic orbit theory has been used to explain the scarred wave function in the quantum chaos [11–13].

Recently, it has been proposed to use optical devices with identical functional form to extract the information of wave functions in mesoscopic systems [14,15]. In this work, we use an isotropic microchip laser to study the properties of the high-order wave functions in a 2D isotropic harmonic oscillator. Experimental results show that the spontaneous high-order patterns are generally the elliptic or hyperbolic modes corresponding to the classical trajectories. The elliptic modes are found to be analogous to the SU(2) coherent states of the 2D quantum harmonic oscillator. The hyperbolic modes are found to be the interference of two identical HG modes with a particular angle θ_p. Theoretical analyses indicate that the angle θ_p corresponds to the local minimum of the transverse mode area.

II. EXPERIMENTAL RESULTS

Figure 1 shows the schematic and the pump profile for the present laser system. The experimental laser cavity consists of one planar Nd:YVO_4 surface, high-reflection coated at 1064 nm and high-transmission coated at 809 nm for the pump light to enter the laser crystal, and a spherical output mirror. The gain medium in the experiment is a *c* cut 2.0 at.% 1 mm length Nd:YVO_4 microchip crystal. It is worthwhile to note that a *c*-cut Nd:YVO_4 crystal is used to realize an isotropic spherical cavity. The YVO_4 crystal belongs to the group of oxide compounds crystallizing in a Zircon structure with tetragonal space group. The fourfold symmetry axis is the crystallographic *c* axis. Perpendicular to this axis are the two indistinguishable *a* and *b* axes. The uniaxial Nd:YVO_4 crystal shows strong polarization-dependent fluorescence emission due to the anisotropic crys-

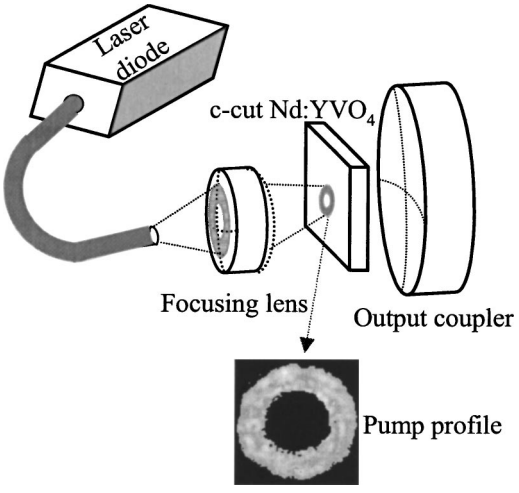

FIG. 1. Schematic of a fiber-coupled diode end-pumped isotropic microchip laser; a typical pump profile of a fiber-coupled laser diode away from the focal plane.

tal field. In a Nd:YVO_4 crystal, for example, the stimulated emission cross section parallel to the c axis, $\sigma_{\parallel}=25\times10^{-19}$ cm^2, is four times higher than that orthogonal to the c axis, $\sigma_{\perp}=6.5\times10^{-19}$ cm^2, for the emission wavelength at 1064 nm [16]. A larger stimulated emission cross section, as usual, results in a lower pumping threshold for laser operation. Therefore, the conventional Nd:YVO_4 crystals are cut along the a axis, i.e., the so-called a cut, to use the stimulated emission cross section of $\sigma_{\parallel}$ to dominate the laser oscillation. To obtain an isotropic stimulated emission cross section in the transverse plane, however, the Nd:YVO_4 crystal should be cut along the c axis, i.e., the so-called c cut.

We setup the resonator length to be as short as possible for reaching single-longitudinal mode operation. The total length in the present resonator is ~2.5 mm. The frequency spacing between consecutive longitudinal modes $\Delta\nu_L$ is about 60 GHz. On the other hand, the transverse mode spacing for the present cavity is given by

$$\Delta\nu_T=\Delta\nu_L\left[\frac{1}{\pi}\cos^{-1}\left(\sqrt{1-\frac{L}{R}}\right)\right], \tag{1}$$

where R is the radius of curvature of the output coupler. A large $\Delta\nu_T$ is beneficial to a lasing transverse mode within a frequency-degenerate family. Therefore, we use an output coupler of $R=10$ mm, corresponding to $\Delta\nu_T=10$ GHz, to ensure the lasing transverse modes belonging to a frequency-degenerate family. The pump source is a 1.0-W fiber-coupled laser diode (coherent, F-81-800C-100) with a 0.1 mm of core diameter. Note that the output intensity profile from an ordinary fiber-coupled laser diode is a top-hat distribution. With the special coupling condition, a fiber-coupled laser diode can have a doughnut output profile. It is extremely important to use a doughnut pump profile for controlling the pump region as well as for keeping the cavity isotropic.

First we use an output coupler with the reflectivity of 98% in the laser resonator. The pump spot size is controlled to be nearly 0.2 mm; the intensity of the pump power is approximately 15 W/mm^2; the incident angle of the pump beam is within $\pm5''$ with respect to the longitudinal axis. The size of the observed patterns is in the range of 0.15–0.2 mm. Near lasing threshold, the laser emits elliptic modes with the standing waves in the azimuthal direction. The order of the elliptic mode can be easily varied by controlling the pump size. The eccentricity of the lasing elliptical mode mainly depends on the spot size and incident angle of the pump beam. The measurement of the optical spectrum reveals that the elliptical mode is a single frequency emission. Figure 2 shows two typical experimental results for the near-field transverse pattern on the concave mirror.

Increasing the reflectivity of the output coupler to 99%, we generally observe the transverse pattern near lasing threshold to be localized on the hyperbolic trajectories. With the center of the pump beam at the longitudinal axis, the persistent patterns are usually the hyperbolic modes. However, the lasing mode may change to the elliptic patterns when the pump beam is off-axis by 20–40 μm. Although the eccentricity of the elliptic modes can be slightly varied by controlling the pump condition, the lasing mode never becomes a circle pattern; that is, the eccentricity cannot go to zero. Similar to the elliptic modes, the order and the shape of the hyperbolic modes mainly depend on the spot size and incident angle of the pump beam. Figures 3(a) and (b) show two typical experimental results for the near-field transverse patterns on the concave mirror. The hyperbolic mode is also measured to be a single frequency emission. Slightly increasing the pump power, the transverse mode displays a coexisting pattern that consists of an elliptic mode and an inscribed hyperbolic mode, as shown in Fig. 3(c). It is found that the coexisting pattern is also a single frequency emission. Moreover, both the elliptic and hyperbolic patterns are linearly polarized and are preserved in free-space propagation. It is well known that only HG modes remain HG field patterns as they propagate. Therefore, the formation of the elliptic and hyperbolic patterns can be interpreted as a spontaneous process of transverse mode locking of degenerate HG modes. To our knowledge, the elliptic and hyperbolic modes are experimentally observed in laser systems.

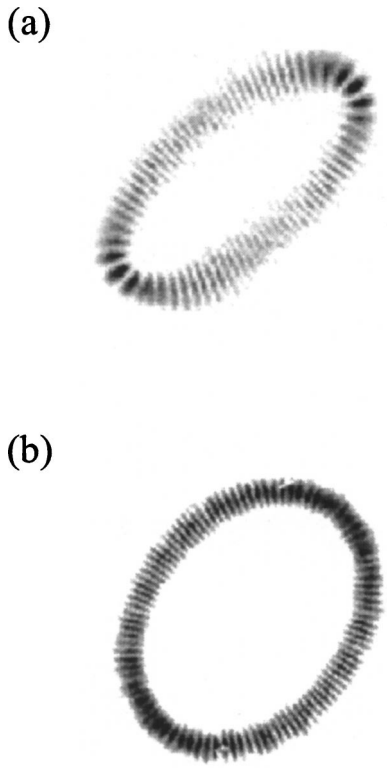

FIG. 2. Typical experimental results for the elliptic transverse patterns near lasing threshold.

The power intensity spectra reveal that both the elliptic and hyperbolic modes display self-sustained relaxation oscillation. In class-B lasers, relaxation oscillations arise from the energy coupling between field and inversion because of the slowness of population inversion. Therefore, the self-sustained relaxation oscillation is the dynamic characteristics of the class-B laser in a single-mode operation; the present results confirm this property.

III. THEORETICAL ANALYSIS

It is well recognized that the classical Hamiltonian of 2D isotropic harmonic oscillator can be simply expressed in

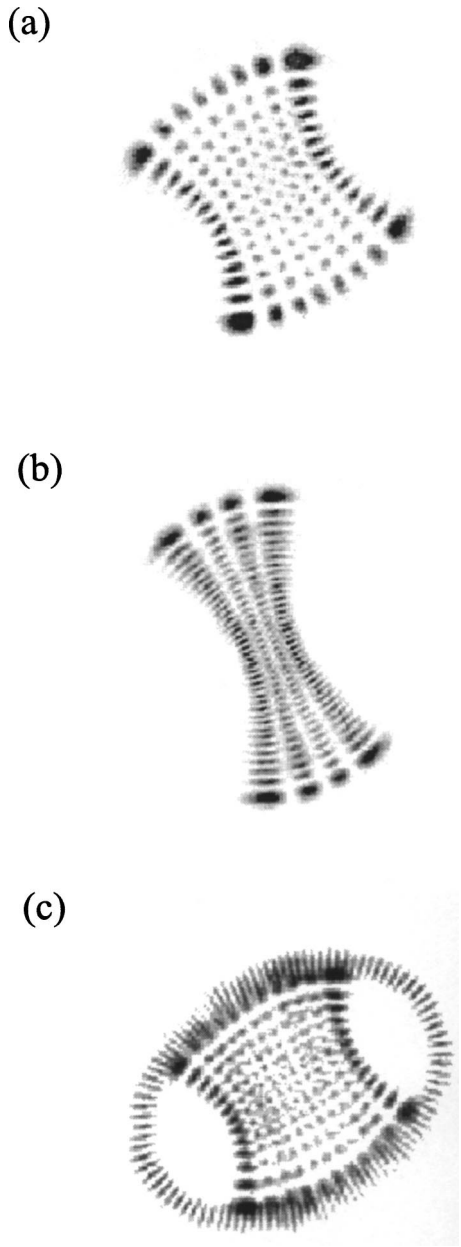

FIG. 3. Typical experimental results for the hyperbolic and coexisting patterns. (a) and (b) Pump power near lasing threshold; (c) pump power at 1.2 times lasing threshold.

terms of the generators of its dynamical group SU(2) [17]. Pollet *et al.* [18] demonstrated that the geometric discussion of the classical meaning of these quantities leads, in the quantum counterpart, to the construction of the SU(2) coherent states, which are well localized on the corresponding classical elliptical trajectories. Results concerning the construction and properties can be essentially found from Ref. [19]. Based on the numerical calculations, it is found that the elliptic modes shown in Fig. 2 are analogous to the SU(2) wave packet of a 2D harmonic oscillator. As in the Schwinger representation of the SU(2) algebra, the wave function for the elliptic mode is given by [20,21]

$$\Psi_N(x,y;\phi)=\frac{1}{2^{N/2}}\sum_{K=0}^{N}\binom{N}{K}^{1/2}e^{iK\phi}\psi_{K,N-K}(x,y), \quad (2)$$

where $\psi_{m,n}(x,y)$ is the HG eigenmode for the spherical resonator [2]:

$$\psi_{m,n}(x,y)=\frac{1}{\sqrt{2^{m+n-1}\pi m!n!}}\frac{1}{\omega_o}H_m\left(\frac{\sqrt{2}x}{\omega_o}\right)H_n\left(\frac{\sqrt{2}y}{\omega_o}\right)\times\exp\left[-\frac{(x^2+y^2)}{\omega_o^2}\right], \quad (3)$$

where ω_o is the laser beam waist. The HG transverse mode is equivalent to the eigenfunction of the 2D quantum harmonic oscillator using the relationship $\omega_o^2=2\hbar/(m\omega)$, where m is the oscillator mass and ω is the angular frequency. For high-order modes, the parameter ϕ in Eq. (2) can be related to the eccentricity of the trajectory e by $e=2\sqrt{\cos\phi}/(1+\cos\phi)$, where $0\leqslant\phi\leqslant\pi/2$. The wave function given in Eq. (2) represents a traveling-wave property. The standing-wave representations can be obtained by replacing the factor $e^{ik\phi}$ with $\sin(K\phi)$ or $\cos(K\phi)$. Including the normalization constant, the standing-wave form for $\cos(K\phi)$ can be written as

$$\Psi_N^c(x,y;\phi)=\frac{1}{\left[\Sigma_{K=0}^{N}\binom{N}{K}\cos^2(K\phi)\right]^{1/2}}\times\sum_{K=0}^{N}\binom{N}{K}^{1/2}\cos(K\phi)\psi_{K,N-K}(x,y). \quad (4)$$

Using Eq. (4), the patterns shown in Fig. 2 were numerically reconstructed, as depicted in Fig. 4. The good agreement between experimental and reconstructed patterns confirms that the observed elliptic modes are analogous to the SU(2) wave packet of a 2D harmonic oscillator.

To interpret the hyperbolic mode, we consider the superposition of two identical HG modes with an arbitrary angle. Due to the isotropic property of the 2D harmonic oscillator, a HG mode under an arbitrary rotation by an angle θ is still an eigenfunction. Namely, the wave function $\psi_{m,n}(x',y')$ is still the eigenfunction of the 2D harmonic oscillator, where $x'=x\cos\theta+y\sin\theta$ and $y'=-x\sin\theta+y\cos\theta$. The completeness of the eigenfunctions of an Hermitian operator warrant that the wave function $\psi_{m,n}(x',y')$ can be in terms of the degenerate eigenstates $\psi_{K,N-K}(x,y)$, where $N=m+n$ and $K=0,1,2,...N$. Using the creation and annihilation operators and various identities known from the angular-momentum theory [22], after tedious algebra, $\psi_{m,n}(x',y')$ can be analytically expressed as

$$\psi_{m,n}(x',y')=\sum_{K=0}^{N}B_K(\theta)\psi_{K,N-K}(x,y), \quad (5)$$

where $B_K(\theta)$ can be in terms of the Wigner d function [22]:

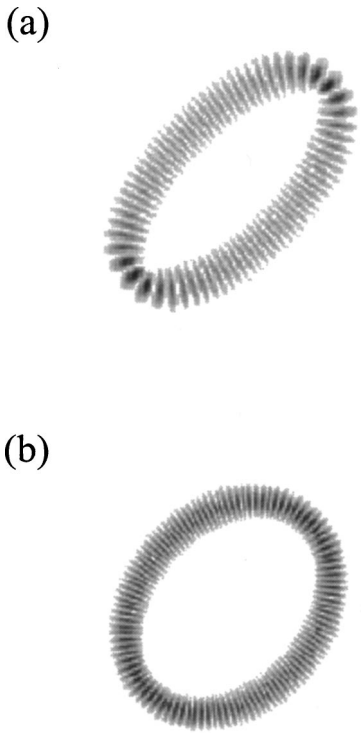

FIG. 4. The theoretically SU(2) elliptic standing waves corresponding to the results shown in Fig. 2. (a) $\Psi^{c}_{35}(x,y;50°)$; (b) $\Psi^{c}_{53}(x,y;75°)$.

$$B_K(\theta) = d^{N/2}_{(N/2)-m,(N/2)-K}(2\theta) = \sqrt{m!(N-m)!K!(N-K)!}\sum_{\nu}(-1)^{\nu} \times \frac{(\cos\theta)^{N-2\nu+K-m}(\sin\theta)^{2\nu+m-K}}{\nu!(N-m-\nu)!(K-\nu)!(m-K+\nu)!}, \quad (6)$$

where the summation over ν is taken whenever none of the arguments of factorials in the denominator are negative.

Using Eqs. (5) and (6), the wave packet for the superposition of two identical HG modes of $\psi_{m,n}(x,y)$ and $\psi_{m,n}(x',y')$ can be written as

$$\Phi_{m,N-m}(x,y;\theta) = \psi_{m,N-m}(x,y) + \psi_{m,N-m}(x',y') = \sum_{K=0}^{N}[B_K(\theta)+\delta_{m,K}]\psi_{K,N-K}(x,y). \quad (7)$$

Here we replace the subscript index n by $N-m$ for convenient presentation. For stable stationary wave patterns, the angle θ of the wave function $\Phi_{m,N-m}(x,y;\theta)$ is governed by the criterion of the minimum threshold pump power. The threshold pump power for the transverse mode $\Phi_{m,N-m}(x,y;\theta)$ can be given by [23]

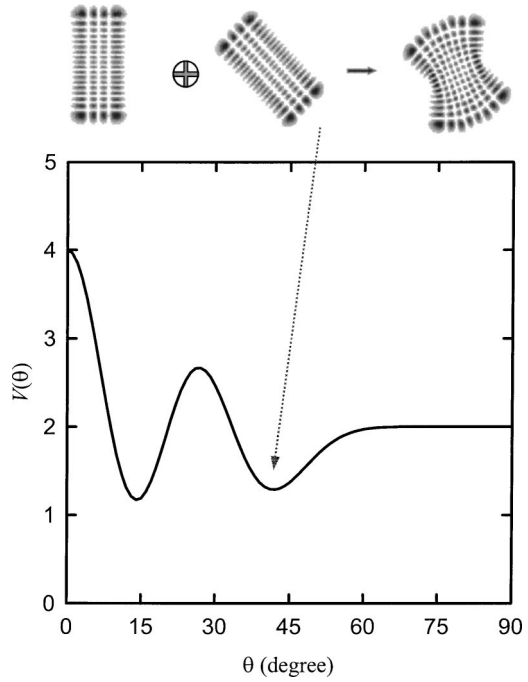

FIG. 5. The mode-area functional $V(\theta)$ as a function of θ for the state $\Phi_{17,3}(x,y;\theta)$. The numerically reconstructed pattern at the local minimum pointed to by the arrow corresponds to the experimental result shown in Fig. 3(a).

$$P_{\mathrm{th}}(\theta) = \frac{\gamma I_{sat}}{\eta_p}\frac{1}{\int\int S(x,y;\theta)R_p(x,y)dxdy}, \quad (8)$$

where γ is the total logarithmic loss per pass, I_{sat} is the saturation intensity, and η_P is the pump efficiency, $R_p(x,y)$ is the normalized pumping distribution, and the normalized intensity distribution $S(x,y;\theta)$ is given by

$$S(x,y;\theta) = \frac{|\Phi_{m,N-m}(x,y;\theta)|^2}{\int_{-\infty}^{\infty}dy\int_{-\infty}^{\infty}dx|\Phi_{m,N-m}(x,y;\theta)|^2}. \quad (9)$$

Substituting Eq. (9) into Eq. (8), the threshold pump power for $\Phi_{m,N-m}(x,y;\theta)$ can be written as

$$P_{\mathrm{th}}(\theta) = \frac{\gamma I_{sat}}{\eta_p}V(\theta)\left[\frac{1}{\int\int|\Phi_{m,N-m}(x,y;\theta)|^2R_p(x,y)dxdy}\right], \quad (10)$$

where the mode-area function $V(\theta)$ is defined as

$$V(\theta) = \int_{-\infty}^{\infty}dy\int_{-\infty}^{\infty}dx|\Phi_{m,N-m}(x,y;\theta)|^2. \quad (11)$$

Numerical calculations confirm that the value of the integration in the square bracket of Eq. (10) is nearly independent of θ because the present pump profile is cylindrically symmetric. Therefore, the minimum mode area corresponds to the minimum pump threshold. Substituting Eq. (7) into Eq. (11) and using the orthonormal property, the functional $V(\theta)$ becomes

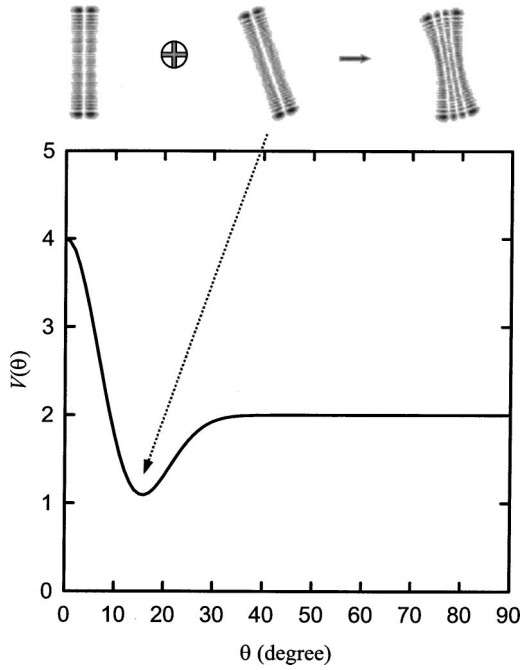

FIG. 6. The mode-area functional $V(\theta)$ as a function of θ for the state $\Phi_{39,1}(x,y;\theta)$. The numerically reconstructed pattern at the local minimum pointed by the arrow corresponds to the experimental result shown in Fig. 3(b).

$$V(\theta)=\sum_{K=0}^{N}|B_K(\theta)+\delta_{m,K}|^2. \tag{12}$$

The local minima of $V(\theta)$ correspond to the transverse patterns near lasing threshold. It is interesting to note that the local minima of the functional $V(\theta)$ for high-order mode physically coincide with the local minima of mode area, compatible with the uncertainty relations for the coherent state.

Figure 5 shows the mode-area functional $V(\theta)$ as a function of θ for the state $\Phi_{17,3}(x,y;\theta)$. One of two local minima is found to correspond to the wave pattern localized on hyperbolic trajectory. It can be seen that the theoretical wave pattern agrees very well with the experimental pattern shown in Fig. 3(b). Note that the wave pattern corresponding to the other local minimum was not excited due to higher lasing threshold. The lasing threshold essentially depends on the pump profile. For a doughnut-shaped pump profile, the elliptic and hyperbolic wave patterns usually have lower lasing threshold than the patterns corresponding to other local minima of the mode area. This is the reason why the high-order transverse patterns observed here are usually localized on classical trajectories. Figure 6 shows the mode-area functional $V(\theta)$ as a function of θ for the state $\Phi_{39,1}(x,y;\theta)$. Once again, the wave corresponding to the local minimum is in good agreement with the experimental pattern shown in Fig. 3(a).

IV. CONCLUSION

A new type of laser transverse modes has been observed in an isotropic microchip laser pumped by using a doughnut pump profile. The observed transverse modes include elliptic and hyperbolic wave patterns that are analogous to the quantum states of classical trajectories of a 2D harmonic oscillator. The elliptic mode is found to be analogous to the SU(2) wave packet of a 2D harmonic oscillator. The hyperbolic mode is found to be a spontaneous mode locking between two identical Hermite-Gaussian modes with a particular angle governed by the minimum mode area. The present results support the idea that the optical devices can be deliberately designed to simulate the quantum phenomenon in mesoscopic physics [14,15]. Recently, Doya *et al.* [24,25] have also introduced the paraxial approximation to establish an analogy between light propagation along a multimode fiber and quantum confined systems. We believe that these analogies will continue to be exploited for understanding the physics of mesoscopic systems.

ACKNOWLEDGMENT

The authors thank the National Science Council for their financial support of this research under Contract No. NSC-91-2112-M-009-030.

[1] S. Flügge, *Practical Quantum Mechanics* (Springer-Verlag, New York, 1971), p. 107.
[2] H. Kogelnik and T. Li, Proc. IEEE **54**, 1312 (1966).
[3] H. A. Haus, *Waves and Fields in Optoelectronics* (Prentice-Hall, Englewood Cliffs, NJ, 1984).
[4] A. E. Siegman, *Lasers* (University Science Books, Mill Valley, CA, 1986).
[5] Y. F. Chen, T. M. Huang, C. F. Kao, C. L. Wang, and S. C. Wang, IEEE J. Quantum Electron. **33**, 1025 (1997).
[6] H. Laabs and B. Ozygus, Opt. Laser Technol. **28**, 213 (1996).
[7] Y. F. Chen and Y. P. Lan, Phys. Rev. A **63**, 063807 (2001).
[8] J. P. Bird, R. Akis, D. K. Ferry, D. Vasileska, J. Cooper, Y. Aoyagi, and T. Sugano, Phys. Rev. Lett. **82**, 4691 (1999).
[9] Y. H. Kim, M. Barth, H. J. Stöckmann, and J. P. Bird, Phys. Rev. B **65**, 165317 (2002).
[10] I. V. Zozoulenko and K. F. Berggren, Phys. Rev. B **56**, 6931 (1997).
[11] M. V. Berry, Proc. R. Soc. London, Ser. A **423**, 219 (1989).
[12] E. B. Bogomolny, Physica D **31**, 169 (1988).
[13] O. Agam and S. Fishman, Phys. Rev. Lett. **73**, 806 (1994).
[14] D. Dragoman and M. Dragoman, Prog. Quantum Electron. **23**, 131 (1999).
[15] D. Dragoman, J. Appl. Phys. **88**, 1 (2000).
[16] H. Nagamoto, M. Nakatsuka, K. Naito, M. Yamanaka, K. Yoshida, T. Sasaki, T. Kanabe, A. Nakai, S. Saito, and Y. Kuwano, Laser Res. **18**, 87 (1990).
[17] H. Goldstein, *Classical Mechanics*, 2nd ed. (Addison-Wesley, Reading, MA, 1980).

[18] J. Pollet, O. Méplan, and C. Gignoux, J. Phys. A **28**, 7282 (1995).
[19] A. Perelomov, *Generalized Coherent States and Their Applications* (Springer-Verlag, Berlin, 1986).
[20] V. Bužek and T. Quang, J. Opt. Soc. Am. B **6**, 2447 (1989).
[21] J. Banerji and G. S. Agarwal, Opt. Express **5**, 220 (1999).
[22] D. A. Varshalovich, A. N. Moskalev, and V. K. Khersonskil, *Quantum Theory of Angular Momentum* (World Scientific, Singapore, 1988).
[23] K. Kubodera and K. Otsuka, J. Appl. Phys. **50**, 653 (1979).
[24] V. Doya, O. Legrand, F. Mortessagne, and C. Miniatura, Phys. Rev. Lett. **88**, 014102 (2002).
[25] V. Doya, O. Legrand, F. Mortessagne, and C. Miniatura, Phys. Rev. E **65**, 056223 (2002).